

## Prompt muon-induced fission: a probe for nuclear energy dissipation

Volker E. Oberacker

Department of Physics & Astronomy, Vanderbilt University,  
Nashville, TN 37235, USA, E-mail: volker.e.oberacker@vanderbilt.edu

*Received 1 January 1999*

**Abstract.** We solve the time-dependent Dirac equation for a muon which is initially bound to a fissioning actinide nucleus. The computations are carried out on a 3-D cartesian lattice utilizing the Basis-Spline collocation method. The muon dynamics is sensitive to the nuclear energy dissipation between the outer fission barrier and the scission point. From a comparison with experimental data we find a dissipated energy of about 10 MeV and a fission time delay due to friction of order  $2 \times 10^{-21}$  s.

*Keywords:* fission reactions, mesonic atoms and molecules, computational techniques

*PACS:* 25.85.-w, 36.10Gv, 02.70.-c

### 1. Introduction

There are two different mechanisms that contribute to nuclear energy dissipation, i.e. the irreversible transfer of energy from collective into intrinsic single-particle motion: two-body collisions and “one-body friction”. The latter is caused by the moving walls of the self-consistent nuclear mean field. The role played by these two dissipation mechanisms in fission and heavy-ion reactions is not yet completely understood. In a pioneering article that appeared in 1976 Davies, Sierk and Nix [1] calculated the effect of viscosity on the dynamics of fission. Assuming that friction is caused by two-body collisions they extracted a viscosity coefficient  $\mu = 0.015$  Tera Poise from a comparison of theoretical and experimental values for the kinetic energies of fission fragments. The corresponding time delay for the nuclear motion from the saddle to the scission point was found to be of order  $\Delta t = 1 \times 10^{-21}$  s. However, in one-body dissipation models the time delay is an order of magnitude

larger. Several experimental techniques are sensitive to the energy dissipation in nuclear fission. At high excitation energy, the multiplicity of pre-scission neutrons [2] or photons [3] depends on the dissipation strength. At low excitation energy, the process of prompt muon-induced fission [4] provides a suitable “clock”. This process will be discussed here.

After muons have been captured into high-lying single particle states they form an excited muonic atom. Inner shell transitions may proceed without photon emission by inverse internal conversion, i.e. the muonic excitation energy is transferred to the nucleus. In actinides, the  $2p \rightarrow 1s$  and the  $3d \rightarrow 1s$  muonic transitions result in excitation of the nuclear giant dipole and giant quadrupole resonance, respectively, which act as doorway states for fission. The nuclear excitation energy is typically between 6.5 and 10 MeV. Most importantly, the muon is still available following these atomic transitions (in the ground state of the muonic atom) and can be utilized to probe the fission dynamics. Eventually though, the muon will disappear as a result of the weak interaction (nuclear capture by one of the fission fragments). However, the nuclear capture occurs on a time scale of order  $10^{-7}$  s which is many orders of magnitude larger than the time scale of fission.

The prompt muon-induced fission process is most easily understood via a “correlation diagram”, i.e. one plots the single-particle energies of the transient muonic molecule as a function of the internuclear distance [5]. If there is a large amount of friction during the motion from the outer fission barrier to the scission point the muon will remain in the lowest molecular energy level  $1s\sigma$  and emerge in the  $1s$  bound state of the *heavy* fission fragment. If, on the other hand, friction is small and hence the nuclear collective motion is relatively fast there is a nonvanishing probability that the muon may be transferred to higher-lying molecular orbitals, e.g. the  $2p\sigma$  level, from where it will end up attached to the *light* fission fragment. Therefore, theoretical studies of the muon-attachment probability to the light fission fragment,  $P_L$ , in combination with experimental data can be utilized to analyze the dynamics of fission, and nuclear energy dissipation in particular.

## 2. Theoretical Developments

Because the nuclear excitation energy in muon-induced fission exceeds the fission barrier height it is justified to treat the fission dynamics classically (no barrier tunneling). For simplicity, we describe the fission path by one collective coordinate  $R$ ; the classical collective nuclear energy has the form

$$E_{\text{nuc}} = \frac{1}{2}B(R)\dot{R}^2 + V_{\text{fis}}(R) + E_{\mu}(R). \quad (1)$$

We utilize a coordinate dependent mass parameter [5] and an empirical double-humped fission potential  $V_{\text{fis}}(R)$  [6] which is smoothly joined with the Coulomb potential of the fission fragments at large  $R$ . The last term in Eq. (1) denotes the instantaneous muonic binding energy which depends on the fission coordinate; this term will be defined later.

To account for the nuclear energy dissipation between the outer fission barrier and the scission point, we introduce a friction force which depends linearly on the velocity. In this case, the dissipation function  $D$  is a simple quadratic form in the velocity

$$\dot{E}_{\text{nuc}}(t) = -2D = -f\dot{R}^2(t). \quad (2)$$

The adjustable friction parameter  $f$  determines the dissipated energy; it is the only unknown quantity in the theory.

For the dynamical description of the muonic wavefunction during prompt fission, the electromagnetic coupling between muon and nucleus ( $-e\gamma_\mu A^\mu$ ) is dominant; the weak interaction is negligible. Because of the nonrelativistic motion of the fission fragments the electromagnetic interaction is dominated by the Coulomb interaction

$$A^0(\mathbf{r}, t) = \int d^3r' \frac{\rho_{\text{nuc}}(\mathbf{r}', t)}{|\mathbf{r} - \mathbf{r}'|}. \quad (3)$$

The muonic binding energy in the ground state of an actinide muonic atom amounts to 12 percent of the muonic rest mass; hence nonrelativistic calculations, while qualitatively correct, are limited in accuracy. Several theory groups have demonstrated the feasibility of such calculations [4, 7, 8] which are based on the time-dependent Schrödinger equation

$$\left[-\frac{\hbar^2}{2m}\nabla^2 - eA^0(\mathbf{r}, t)\right] \psi(\mathbf{r}, t) = i\hbar \frac{\partial}{\partial t} \psi(\mathbf{r}, t). \quad (4)$$

Recently, we have developed a numerical algorithm to solve the relativistic problem on a three-dimensional Cartesian mesh [9, 5]. The time-dependent Dirac equation for the muonic spinor wave function in the Coulomb field of the fissioning nucleus has the form

$$H_{\text{D}}(t) \psi(\mathbf{r}, t) = i\hbar \frac{\partial}{\partial t} \psi(\mathbf{r}, t), \quad (5)$$

where the Dirac Hamiltonian is given by

$$H_{\text{D}}(t) = -i\hbar c\boldsymbol{\alpha} \cdot \nabla + \beta mc^2 - eA^0(\mathbf{r}, t). \quad (6)$$

Our main task is the solution of the Dirac equation for the muon in the presence of a time-dependent external Coulomb field  $A^0(\mathbf{r}, t)$  which is generated by the fission fragments in motion. Note the coupling between the fission dynamics, Eq. (1), and the muon dynamics, Eq. (5), via the instantaneous muonic binding energy

$$E_\mu(R(t)) = \langle \psi(\mathbf{r}, t) | H_{\text{D}}(t) | \psi(\mathbf{r}, t) \rangle \quad (7)$$

which depends on the fission coordinate; the presence of this term increases the effective fission barrier height.

### 3. Lattice Representation: Basis-Spline Expansion

For the numerical solution of the time-dependent Dirac equation (5) it is convenient to introduce dimensionless space and time coordinates

$$\begin{aligned} \mathbf{x} &= \mathbf{r}/\lambda_c & \lambda_c &= \hbar/(m_\mu c) = 1.87 fm \\ \tau &= t/\tau_c & \tau_c &= \lambda_c/c = 6.23 \times 10^{-24} s \end{aligned} \quad (8)$$

where  $\lambda_c$  denotes the reduced Compton wavelength of the muon and  $\tau_c$  the reduced Compton time. For the lattice representation of the Dirac Hamiltonian and spinor wave functions we introduce a 3-dimensional rectangular box with a uniform lattice spacing  $\Delta x$ . The lattice points are labeled  $(x_\alpha, y_\beta, z_\gamma)$ .

Our numerical algorithm is the Basis-Spline collocation method [10]. Basis-Spline functions  $B_i^M(x)$  are piecewise-continuous polynomials of order  $(M - 1)$ . These may be thought of as generalizations of the well-known ‘‘finite elements’’ which are a B-Splines with  $M = 2$ . To illustrate the method let us consider a wave function which depends on one space coordinate  $x$ ; we represent the wave function on a finite spatial interval as a linear superposition of B-Spline functions

$$\psi(x_\alpha) = \sum_{i=1}^N B_i^M(x_\alpha) c^i. \quad (9)$$

In the Basis-Spline collocation method, local operators such as the EM potential  $A^0$  in Eq. (6) become diagonal matrices of their values at the grid points (collocation points), i.e.  $V(x) \rightarrow V_\alpha = V(x_\alpha)$ . The matrix representation of derivative operators is more involved [10]. For example, the first-derivative operator of the Dirac equation has the following matrix representation on the lattice

$$D_\alpha^\beta \equiv \sum_{i=1}^N B'_{\alpha i} B^{i\beta}, \quad (10)$$

where  $B'_{\alpha i} = [dB_i^M(x)/dx]|_{x=x_\alpha}$ . Furthermore, we use the shorthand notation  $B_{\beta i} = B_i^M(x_\beta)$  for the B-spline function evaluated at the collocation point  $x_\beta$ , and the inverse of this matrix is denoted by  $B^{i\beta} = [B^{-1}]_{\beta i}$ . Because of the presence of this inverse, the operator  $D_\alpha^\beta$  will have a nonsparse matrix representation. In the present calculations we employ B-Splines of order  $M = 5$ . Eq. (9) can readily be generalized to three space dimensions; in this case the four Dirac spinor components  $\psi^{(p)}$ ,  $p = (1, \dots, 4)$  are expanded in terms of a product of Basis-Spline functions

$$\psi^{(p)}(x_\alpha, y_\beta, z_\gamma, t) = \sum_{i,j,k} B_i^M(x_\alpha) B_j^M(y_\beta) B_k^M(z_\gamma) c_{(p)}^{ijk}(t), \quad (11)$$

i.e. the lattice representation of the spinor wave function is a vector with  $N = 4 \times N_x \times N_y \times N_z$  complex components. Hence, it is impossible to store  $H_D$  in

memory because this would require the storage of  $N^2$  complex double-precision numbers. We must therefore resort to iterative methods for the solution of the matrix equation which do not require the storage of  $H_D$ .

We solve the time-dependent Dirac equation in two steps: first, we solve the static Coulomb problem at time  $t = 0$ , i.e. the muon bound to an actinide nucleus. This problem is solved by the damped relaxation method [5]. The second part of our numerical procedure is the solution of the time-dependent Dirac equation (5) by a Taylor-expansion of the propagator for an infinitesimal time step  $\Delta t$ . Details may be found in ref. [5].

#### 4. Discussion of Numerical Results

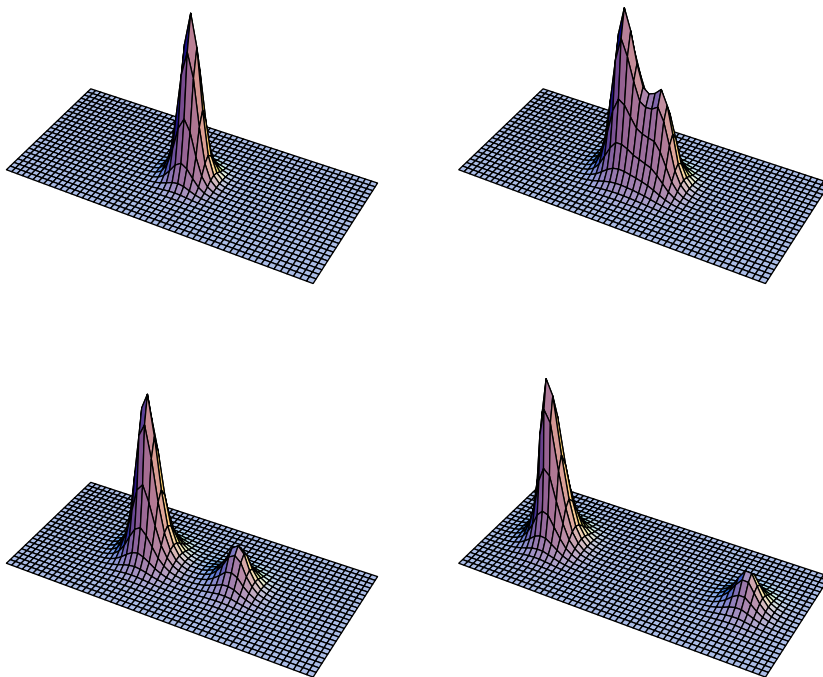
In the following we present results for prompt fission of  $^{237}_{93}\text{Np}$  induced by the  $3d \rightarrow 1s$  muonic transition (9.5MeV). All results reported here are for a 3-D Cartesian lattice of size  $L_x = L_y = 67$  fm and  $L_z = 146$  fm with  $N_x \times N_y \times N_z = 25 \times 25 \times 53$  lattice points with a uniform lattice spacing  $\Delta x = 1.5\lambda_c = 2.8$  fm. Depending on the value of the friction coefficient, we utilize between 1,200–1,900 time steps with a step size  $\Delta t = 1.5\tau_c = 9.3 \times 10^{-24}$  s. Typical production runs take about 11 hours of CPU time on a CRAY supercomputer or about 54 hours on an IBM RS/6000 workstation.

Fig. 1 shows the time-development of the muon position probability density during fission at a fragment mass asymmetry  $\xi = A_H/A_L = 1.10$ . As expected, the muon sticks predominantly to the heavy fragment, but for this small mass asymmetry the muon attachment probability to the light fission fragment,  $P_L$ , is rather large (20 percent).

One might ask whether the muon will always remain bound during fission; what is the probability for ionization? To investigate this question we have plotted the muon position probability density on a logarithmic scale.

In coordinate space, any appreciable muon ionization would show up as a “probability cloud” that is separating from the fission fragments and moving towards the boundaries of the lattice. Fig. 2 shows no evidence for such an event in our numerical calculations. Hence, we conclude that the probability for muon ionization  $P_{\text{ion}}$  is substantially smaller than the muon attachment probability to the light fission fragment which is always clearly visible in our logarithmic plots, even at large mass asymmetry. From this we estimate that  $P_{\text{ion}} < 10^{-4}$ .

Fig. 3 shows that  $P_L$  depends strongly on the fission fragment mass asymmetry. This is easily understood: for equal fragments we obviously obtain  $P_L = 0.5$ , and for large mass asymmetry it is energetically favorable for the muon to be bound to the heavy fragment, hence  $P_L$  will be small. In Fig. 3 we also examine the dependence of  $P_L$  on the dissipated nuclear energy,  $E_{\text{diss}}$ , during fission. In our model, friction takes place between the outer fission barrier and the scission point. When the dissipated energy is computed from equation (2) we find an almost linear dependence of the muon attachment probability on  $E_{\text{diss}}$ ; unfortunately, this dependence is



**Fig. 1.** Prompt muon-induced fission of  $^{237}_{93}\text{Np}$  for a fission fragment mass asymmetry  $\xi = A_H/A_L = 1.10$  at  $E^* = 9.5$  MeV. Shown is the muon position probability density at four different times during fission:  $t = 0$ ,  $6.5 \times 10^{-21}$  s,  $8.4 \times 10^{-21}$  s,  $1.1 \times 10^{-20}$  s. Zero friction ( $f = 0$ ) has been assumed.

rather weak.

We would like to point out that the theoretical values for  $P_L$  obtained in this work are smaller than those reported in our earlier calculations [9, 5]. There are two reasons for this: (a) the size of the lattice and (b) the lattice representation of the first derivative operator in the Dirac equation. Because of constraints in the amount of computer time available to us we utilized a smaller cubic lattice in our prior calculations [5] with  $N_x \times N_y \times N_z = 29^3$  lattice points. More recently, we were able to increase the size of the lattice substantially, in particular in fission ( $z$ -) direction (see above). In Fig. 2 of ref. [11] we have demonstrated the convergence of our results for the muon attachment probability in terms of the lattice size and lattice spacing. Another reason for the difference between the current and prior results is the lattice representation of the first derivative operator, Eq. (10), in the Dirac equation. In ref. [9, 5] we utilized a combination of forward and backward derivatives for the upper and lower spinor wave function components; after extensive testing of Coulomb potential model problems with known analytical solutions we have found that the symmetric derivative operator provides a more faithful lattice

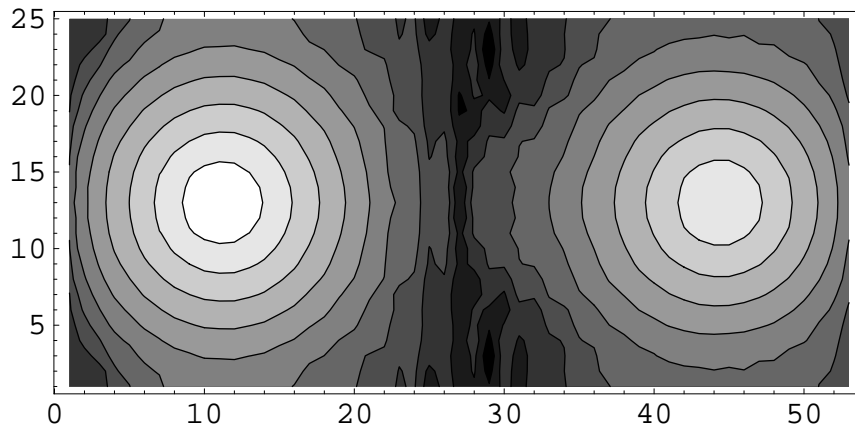


**Fig. 2.** Contour plot of the logarithm of the muon probability density at  $t = 1.1 \times 10^{-20}$  s shows no evidence of muon ionization.

representation. The results reported here and in ref. [11] have been obtained utilizing the symmetric derivative prescription.

## 5. Comparison of Theory with Experiment

There are only a few experimental data available for comparison. Schröder *et al.* [12] measured for the first time mean lifetimes of muons bound to fission fragments of several actinide nuclei. The muon decays from the K-shell of the muonic atom through various weak interaction processes at a characteristic rate  $\lambda = \lambda_0 + \lambda_c$ , where  $\lambda_0 = (2.2 \times 10^{-6} \text{s})^{-1}$  is the free leptonic decay rate for the decay process  $\mu^- \rightarrow e^- + \bar{\nu}_e + \nu_\mu$  and  $\lambda_c$  denotes the nuclear capture rate;  $\lambda_c$  depends upon the charge and mass of the fission fragment. From the observed lifetime  $\tau_\mu = 1.30 \times 10^{-7} \text{s}$  Schröder *et al.* estimated an upper limit for the muon attachment probability  $P_L \leq 0.1$ . It must be emphasized that this number represents an integral over the whole fission mass distribution and, hence, cannot be directly compared to the numbers given in Fig. 3.

The most complete experiments have been carried out by Risse *et al.* [13] at the Paul Scherrer Institute (PSI) in Switzerland. The basic experimental approach is to place a fission chamber inside an electron spectrometer. The incident muons are detected by a scintillation counter. An event is defined by a  $(\mu^-, f_1 f_2 e^-)$  coincidence where the fission fragments are observed in prompt and the muon decay electrons in delayed coincidence with respect to the incident muon. The magnetic field of the electron spectrometer allows for a reconstruction of the electron trajectories. Thus, it is possible to determine whether the muon decay electrons originate from the heavy or the light fission fragment.

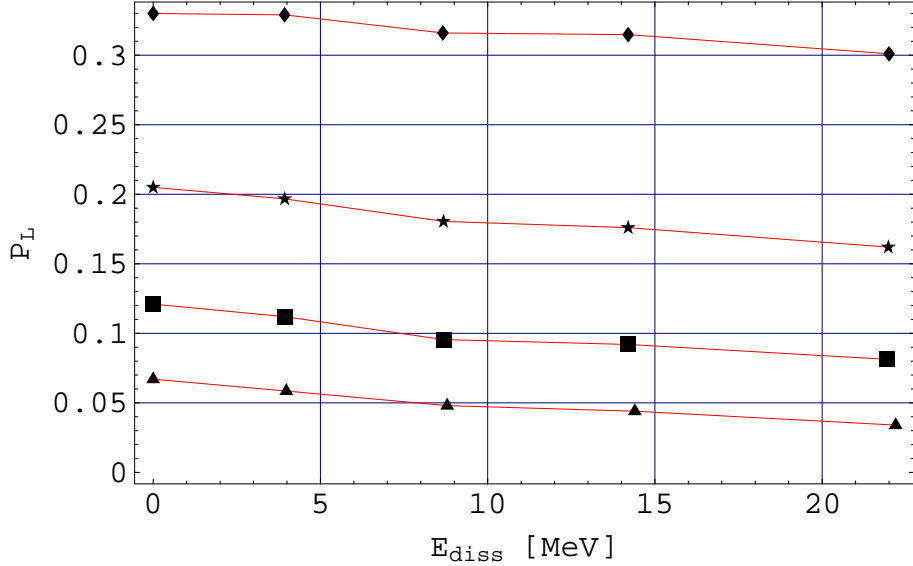


**Fig. 3.** Muon attachment probability to the light fission fragment as function of nuclear energy dissipation for  $^{237}_{93}\text{Np}$ . Results are shown for fragment mass asymmetries  $\xi = 1.05$  (upper curve), 1.10, 1.15, and 1.20 (lower curve).

For several mass bins of the light fission fragment, muon attachment probabilities  $P_L$  have been measured; the experimental data are given in Table 1. It should be emphasized that the mass bins are relatively broad. Because the theoretical values for  $P_L$  depend strongly on the mass asymmetry it is not justified to assume that  $P_L$  remains constant within each experimental mass bin. Instead, to allow for a comparison between theory and experiment, we have to multiply the theoretical  $P_L$  values in Fig. 3 with a weighting factor that accounts for the measured relative mass distribution [13] of the prompt fission events within this mass bin. We subsequently integrate the results over the sizes of the experimental mass bins. Due to the relatively low excitation energy in muon-induced fission, the fission mass distribution exhibits a maximum at  $\xi = A_H/A_L = 1.4$  and falls off rather steeply for values larger or smaller than the maximum. This means that the large values of  $P_L \approx 0.5$  at or near fission fragment symmetry  $\xi = 1.0$  will be strongly suppressed. The resulting theoretical values for  $P_L$  are given in the last column of Table 1. It is apparent that our theory agrees rather well with experiment. Because of the size of the error bars in the experiment and because of the weak dependence of the theoretical values of  $P_L$  on the dissipated energy, it is not possible to extract very precise information about the amount of energy dissipation.

From a comparison of our theoretical result for the mass bin  $A_L = 118.5 \rightarrow$

**Table 1.** Muon-attachment probabilities to the light fission fragment,  $P_L$ , for  $^{237}\text{Np}(\mu^-, f)$ . Exp. data are taken from ref. [13].

mass bin $A_L$	mass asymmetry	$P_L(\text{exp})$	$P_L(\text{theo})$
118.5 $\rightarrow$ 111.5	1.000 $\rightarrow$ 1.126	$(25.5 \pm 8.5) \times 10^{-2}$	$26.0 \times 10^{-2}, E_{\text{diss}} = 0\text{MeV}$ $22.3 \times 10^{-2}, E_{\text{diss}} = 22\text{MeV}$
111.5 $\rightarrow$ 104.5	1.126 $\rightarrow$ 1.268	$(9.7 \pm 2.6) \times 10^{-2}$	$6.62 \times 10^{-2}, E_{\text{diss}} = 0\text{MeV}$ $3.51 \times 10^{-2}, E_{\text{diss}} = 22\text{MeV}$

111.5 with the measured data we extract a dissipated energy of order 10 MeV for  $^{237}\text{Np}$  while the second mass bin  $A_L = 111.5 \rightarrow 104.5$  is more compatible with zero dissipation energy. We place a higher confidence on the theoretical results for the first mass bin because the probabilities  $P_L$  are substantially larger and hence numerically more reliable. We like to point out that our theoretical value  $E_{\text{diss}} = 10$  MeV is compatible with results from other low-energy fission measurements that are based on the odd-even effect in the charge yields of fission fragments [14]. In addition to  $^{237}\text{Np}$  we have also studied muon-induced fission of  $^{238}\text{U}$ ; the results for muon attachment are very similar [11].

## 6. Conclusions

We have studied the dynamics of a muon bound to a fissioning actinide nucleus by solving the time-dependent Dirac equation for the muonic spinor wavefunction; the fission dynamics is described classically. The theory predicts a strong mass asymmetry dependence of the muon attachment probability  $P_L$  to the light fission fragment; this feature is in agreement with experimental data. Our calculations show no evidence for muon ionization during fission. The theory also predicts a (relatively weak) dependence of  $P_L$  on the dissipated energy. By comparing our theoretical results to the experimental data of ref. [13] we extract a dissipated energy of about 10 MeV for  $^{237}\text{Np}$  (see Table 1). Using the dissipation function defined in Eq. (2), this value corresponds to a fission time delay from saddle to scission of order  $2 \times 10^{-21}$  s.

## Acknowledgements

This research project was sponsored by the U.S. Department of Energy under contract No. DE-FG02-96ER40975 with Vanderbilt University. For several years, I have benefitted from fruitful discussions with my collaborators, in particular with

J.A. Maruhn, the late C. Bottcher, M.R. Strayer, P.G. Reinhard, A.S. Umar and J.C. Wells. Some of the numerical calculations were carried out on CRAY supercomputers at NERSC, Berkeley. I also acknowledge travel support to Germany from the NATO Collaborative Research Grants Program.

## References

1. K.T.R. Davies, A.J. Sierk and J.R. Nix, *Phys. Rev. C* **13** (1976) 2385.
2. A. Gavron *et al.*, *Phys. Rev. C* **35** (1987) 579.
3. D.J. Hofmann *et al.*, *Phys. Rev. C* **51** (1995) 2597.
4. J.A. Maruhn, V.E. Oberacker and V. Maruhn-Rezwani, *Phys. Rev. Lett.* **44** (1980) 1576.
5. V.E. Oberacker, A.S. Umar, J.C. Wells, C. Bottcher, M.R. Strayer and J.A. Maruhn, *Phys. Rev. C* **48** (1993) 1297.
6. B.B. Back, *Nucl. Phys.* **A 228** (1974) 323.
7. Z. Ma, X. Wu, J. Zhang, Y. Zhuo and J.O. Rasmussen, *Phys. Lett.* **B106** (1981) 159.
8. F.F. Karpeshin, *Nucl. Phys.* **A 617** (1997) 211.
9. V.E. Oberacker, A.S. Umar, J.C. Wells, C. Bottcher and M.R. Strayer, *Phys. Lett.* **B293** (1992) 270.
10. J.C. Wells, V.E. Oberacker, M.R. Strayer and A.S. Umar, *Int. J. Mod. Phys.* **C6** (1995) 143.
11. V.E. Oberacker, A.S. Umar, J.C. Wells, M.R. Strayer, J.A. Maruhn and P.G. Reinhard, *Proc. Int. Conf. on Fission and Properties of Neutron-Rich Nuclei*, eds J.H. Hamilton and A.V. Ramayya, Sanibel Island, Florida, USA, November 10–15, 1997, World Scientific, Singapore, 1998, p. 395.
12. W.U. Schröder, W.W. Wilcke, M.W. Johnson, D. Hilscher, J. R. Huizenga, J. C. Browne and D. G. Perry, *Phys. Rev. Lett.* **43** (1979) 672.
13. F. Risse, W. Bertl, P. David, H. Hänscheid, E. Hermes, J. Konijn, C.T.A.M. de Laat, H. Pruys, Ch. Rösler, W. Schrieder, A. Taal and D. Vermeulen, *Z. Phys.* **A 339** (1991) 427.
14. C. Wagemans, *The Nuclear Fission Process*, p.418 (CRC Press, Boca Raton, 1991)